

Smart Laser-Writable Micropatterns with Multiscale Photo/Moisture Reconstructible Structure

Songshan Zeng, Yin Liu, Shuliang Li, Kuangyu Shen, Zaili Hou, Aimee P. Chooi, Andrew T. Smith, Zi Chen,* and Luyi Sun*

The design of a dynamic, versatile, convertible, and responsive micropatterned system is realized by a photo/moisture reconstructible multiscale film-substrate bilayer structure. Specifically, a hydrophilic polyvinyl alcohol (PVA)/laponite (LP) thin film is covalently bonded to a photothermally active polydimethylsiloxane (PDMS)/carbon black (CB) soft substrate. A laser engraver can inscribe programmable aligned micro-wrinkles by manipulating laser power and spatiotemporal control. These wrinkles can be modulated into three distinct systems 1) moisture erasable and laser re-writable wrinkles; 2) moisture driven reversible wrinkles; 3) moisture resistant wrinkles, which are achieved by controlling a) the moisture resistance of PVA; b) the dimensional stability of PVA/LP film regulated by the LP nanostructure, which can be adjusted by the laser power and the LP ratio. This programmable system can be applied in information encryption/recording and as a moisture responsive electrical switch, offering new routes for the modulations and applications of next generation smart materials.

serving as environmental camouflage.^[5–8] Additionally, the nano/microscale wrinkling patterns on the petal of gorteria diffusa flower can create intriguing iridescent structural colors.^[9] These versatile topographies have inspired the micro/nano fabrication of analogous smart materials, which demonstrate dynamic responsiveness to external stimuli for numerous applications, including information recording and encryption,^[10,11] strain sensor and actuator,^[12–16] dynamic chromic device,^[17,18] smart adhesion,^[19,20] and soft photonics.^[21–26]

Wrinkles, a mechanical instability created by compressing a rigid thin film attached to a soft substrate, can be generated via various approaches, such as mechanical strain,^[27–30] solvent,^[11] heat,^[31] and light.^[23] Among these, light is widely used, because it is considered a non-con-

1. Introduction


A variety of organisms have evolved to possess various micro-structured surfaces, including cracks, wrinkles, folds, creases, grooves, etc. For instance, both beetles and lizards have groove-like hexagonal micro-textures on their skins, which can direct the flow of water to maximize the water harvest.^[1–4] The dermal layer of cephalopod skin contains micro-structured radial muscles that control the exposure of the underlying chromatophores,

contact, long range, spatiotemporal controllable, and flexible stimulus source with tunable parameters (such as intensity, wavelength, etc.) and scalability. Light induced wrinkled surfaces are commonly fabricated based on photo tunable chemicals, such as azo-based polymers,^[23,32–34] reversible UV crosslinked networks,^[21,35–37] etc. Although decent progress has been achieved, limitations still exist. For example, these light responsive materials require relatively complicated synthesis processes. Moreover, the responsiveness of these light induced wrinkled surfaces to other stimuli, such as moisture, remains largely unexplored. Introduction of additional stimuli allows the system to be much more versatile and adaptable with multi-stimuli responsiveness and will enable wrinkled devices to acquire unprecedented properties and applications. For instance, the tunability of laser induced wrinkles by other stimuli endows a dynamic, interactive, and convertible smart optical system, that can decode various types of stimuli by changes of optical or other wrinkle properties. These responses to multiple stimuli are crucial for the fields of sensor,^[31,38] encryption,^[10,11] smart optics,^[21–23] interactive electronics,^[39] and other advanced materials systems.^[19,20] Also, it offers new routes to further reveal the unexploited wrinkle modulation mechanisms and undeveloped methodology for tuning wrinkle responsive dynamics. Additionally, decoupling the stimuli can give greater control in manipulating each stimulus independently without cross-interference. For example, it is important to apply a different stimulus in addition to light to modulate the wrinkles (such as

Dr. S. Zeng, S. Li, K. Shen, Z. Hou, A. P. Chooi, A. T. Smith, Prof. L. Sun
Department of Chemical and Biomolecular Engineering
and Polymer Program
Institute of Materials Science
University of Connecticut
Storrs, CT 06269, USA
E-mail: luyi.sun@uconn.edu

Dr. Y. Liu, Prof. Z. Chen
Thayer School of Engineering
Dartmouth College
Hanover, NH 03755, USA
E-mail: zi.chen@dartmouth.edu

Prof. L. Sun
Department of Biomedical Engineering
University of Connecticut
Storrs, CT 06269, USA

 The ORCID identification number(s) for the author(s) of this article can be found under <https://doi.org/10.1002/adfm.202009481>.

DOI: 10.1002/adfm.202009481

erase, re-activate), which can avoid unwanted re-generation of wrinkles. Also, other stimulus might be more accessible in certain circumstances. Since moisture is readily available in daily life, such as from human breath, humid air, or wet mist from the natural environment or man-made devices, it can be considered as a ubiquitous and highly accessible stimulus to modulate the responsiveness of the light induced wrinkles. Besides, very few studies have linked the optical properties of wrinkles to other functionalities, like electrical resistance response.^[39] Therefore, it is imperative to introduce a facile method to fabricate new photo/moisture responsive materials to form light induced smart wrinkles with tunable moisture responsiveness, which can be leveraged into new applications with wider scope and multi-functionalities.

2. Results

2.1. Design, Fabrication, and Moisture Responsiveness Modulation Scheme for Laser Engraving (LE) Wrinkles

Herein, we developed a dynamic, versatile, convertible, and responsive micropatterned system based on a photo/moisture reconstructible multiscale hybrid structure. The design consists of a covalently bonded film-substrate structure, where the film is a composite of 2D laponite (LP) nanosheets and hydrophilic polyvinyl alcohol (PVA) matrix, while the substrate is made of a photothermally active polydimethylsiloxane (PDMS)/carbon black (CB). LP nanosheets were incorporated to improve the mechanical strength and dimensional stability of the resultant PVA/LP film without sacrificing transparency,^[40] while CB was introduced to enhance the photothermal effect. A laser engraver can inscribe programmable maskless patterns by controlling the power and scanning rate used, acting as the stimulus to generate wrinkles regionally and tune the nanostructure in the film. Finite element analysis (FEA) was conducted to explore the mechanism of the wrinkle formation. The resultant laser engraving (LE) wrinkles can be tailored into 1) moisture erasable and laser re-writable; 2) moisture driven reversible; 3) moisture resistant. These modulations were achieved by controlling the moisture resistance of the PVA resin, and the dimensional stability of the PVA/LP film regulated by the morphology of the LP nanosheets in the PVA matrix, which can be tuned by the LP concentration and the laser power. These variables collectively and interactively dictate the moisture responsiveness of the LE wrinkles. This dynamic system can be applied for photo/moisture/mechanical responsive information recording/encryption device and moisture responsive electrical switch. Thus, new strategies for modulating the responsive dynamics of wrinkles via multiscale structural design are developed, ranging from selecting PVA molecular structure, tuning the LP nanostructure, to generating micro-scale wrinkling surface. It also further extends the scope of applications for next generation wrinkled devices.

As shown in Figure S1 (Supporting Information), the laser source (wavelength = 450 nm, maximum power = 3.00 W) is fixed on motorized sliders, allowing the laser beam to move in the x and y directions. The laser power, inscribing location, and exposure duration can be precisely controlled by software.

As shown in Figure 1a, to generate a programmable LE wrinkled pattern, the software will set up a designated rectangular area (black dashed line shown in Figure 1a) that covers the preset pattern on the film. The laser power should be carefully regulated so that it can create sufficient photothermal effect to generate wrinkles without burning or melting the PVA/LP thin film, which makes it completely different from other surface destructive engraving processes. During one inscribing cycle, the laser beam only scans in the x direction on the preset patterned area with the predetermined laser power, and switches to the non-engraving mode on the non-patterned area, and then moves in the y direction at the edge of the rectangular area prior to the next inscribing cycle. Since the laser beam only scans along the x direction on the patterned area, it will induce anisotropic compressive stress on the film to generate aligned wrinkles, which will be discussed in detail below. The structures of LP and PVA are shown in Figure 1b. LP is a synthetic phyllosilicate clay with a disc-like 2D shape, and a single-layer LP nanosheet has a typical diameter of 25 to 35 nm and a thickness of 0.92 nm^[40–42] (see Figure S2 (Supporting Information) for a TEM image of the laponite nanosheet). Due to the space confinement effect and evaporation induced orientation of LP nanosheets in the PVA/LP aqueous suspension during the drying process, the LP nanosheets align along the plane direction of the formed film.^[36] Thus, the thickness-wise nanostructure of the PVA/LP film is mainly determined by the ratio of LP to PVA: a higher LP to PVA ratio typically leads to a better nacre-like ordered structure.^[36] PVA chains contain both hydroxyl and acetate side groups. The average molar ratio of the hydroxyl groups to the sum of all side groups on PVA chains is denoted as the degree of hydrolysis (DH). Note that both the crystallinity and the moisture resistance of PVA have a positive correlation with the DH.^[43] Hence, the DH of PVA can strongly influence the moisture responsiveness of the resultant PVA/LP film. Overall, the design of the photo/moisture reconstructible multiscale hybrid structure for fabricating the LE wrinkles with tunable moisture responsiveness should consider the following variables: 1) photothermal active substrate; 2) film and substrate properties required for wrinkle formation; 3) moisture resistance of PVA; 4) ratio of LP to PVA and the corresponding nanostructure in the film; 5) laser power and scanning rate. These variables collectively determine the moisture responsiveness of the LE wrinkles which will be discussed in the following context.

The preparation scheme of this film-substrate bilayer is shown in Figure S3 (Supporting Information). The as-prepared covalently bonded bilayer needs to be carefully peeled from a polystyrene foundation in one direction. This procedure will generate distributed aligned cracks on the brittle PVA/LP films containing a high concentration of LP (40 wt%), while the films containing a low concentration of LP (10 wt%) are sufficiently ductile to remain intact without cracks. To generate LE wrinkles with different moisture responsive dynamics, as shown in Figure 1c, two designs denoted as Sample A and Sample B are prepared. In Sample A, the PVA/LP thin film comprises a low concentration of LP (10 wt%) and partially hydrolyzed PVA (POVAL 8–88) with a low DH of $\approx 88\%$ exhibiting low crystallinity (see Figure S4 in the Supporting Information) and low moisture resistance. The LP nanosheets are

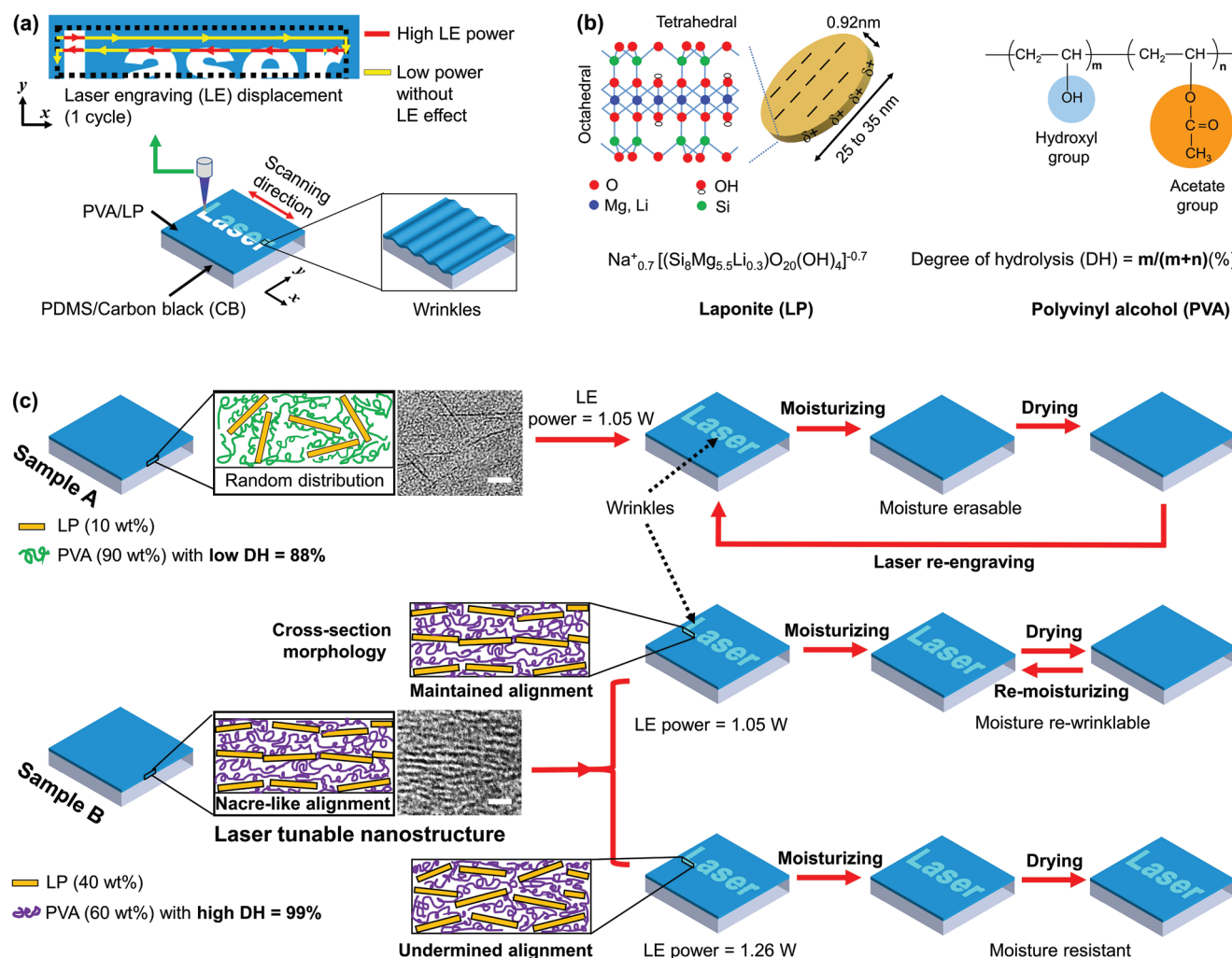


Figure 1. Schematic of the fabrication method, film components, and moisture responsiveness modulation for the laser engraving (LE) wrinkles. a) Inscripting mechanism of laser engraver. b) Chemical structure of laponite (LP) and polyvinyl alcohol (PVA). c) Schematic for tuning the moisture responsive dynamics of the LE wrinkles enabled by modulating the nanoscale architecture with different LP ratios and different laser powers (scale bar = 10 nm).

randomly distributed in the PVA matrix (see the TEM image in Figure 1c), which can effectively enhance the overall mechanical strength under moisturization^[40] (a room temperature mist propelled from a humidifier with a relative humidity (RH) of 100% was used as the moisture source unless otherwise mentioned). A laser power of 1.05 W can generate LE wrinkles, which can be completely erased by moisturization and re-formed by laser, due to the total release of residual stress in the low DH PVA by moisturization.^[11] In Sample B, the film is composed of a higher concentration of LP (40 wt%) and highly hydrolyzed PVA (POVAL 28–99) with a DH of $\approx 99\%$ exhibiting a high crystallinity and moisture resistance (see Figure S4 in the Supporting Information). The high filler concentration allows the LP nanosheets to form a nacre-like nano-architecture as verified by the TEM image in Figure 1c. If Sample B is exposed to a LE power of 1.05 W, the LE wrinkles can be formed concomitant with maintaining a high level of LP alignment, endowing the film with a high dimensional

stability,^[36,44–46] which can introduce shape recovery effect^[46–50] via effectively restricting the motion of PVA chains. Although moisture can only partially release the stress in the high DH PVA, with residual stress remaining, the wrinkles can still be flattened after the first moisturization and subsequent drying cycle, due to the dominance of dimensional stability induced shape recovery effect over residual stress. Upon further moisturization, wrinkles can be re-generated on the original LE area due to the swelling stress and residual stress and become re-flattened after drying. If Sample B undergoes a higher LE power of 1.26 W, the LE wrinkles are still generated. However, the LP alignment and the corresponding dimensional stability will be undermined, and hence the wrinkles follow a similar moisture resistant response to that of the wrinkles on the pure high DH PVA, in which the wrinkles cannot be completely erased even under multiple moisturization/drying cycles as verified by the controlled experiment due to the high moisture resistance of this PVA matrix.

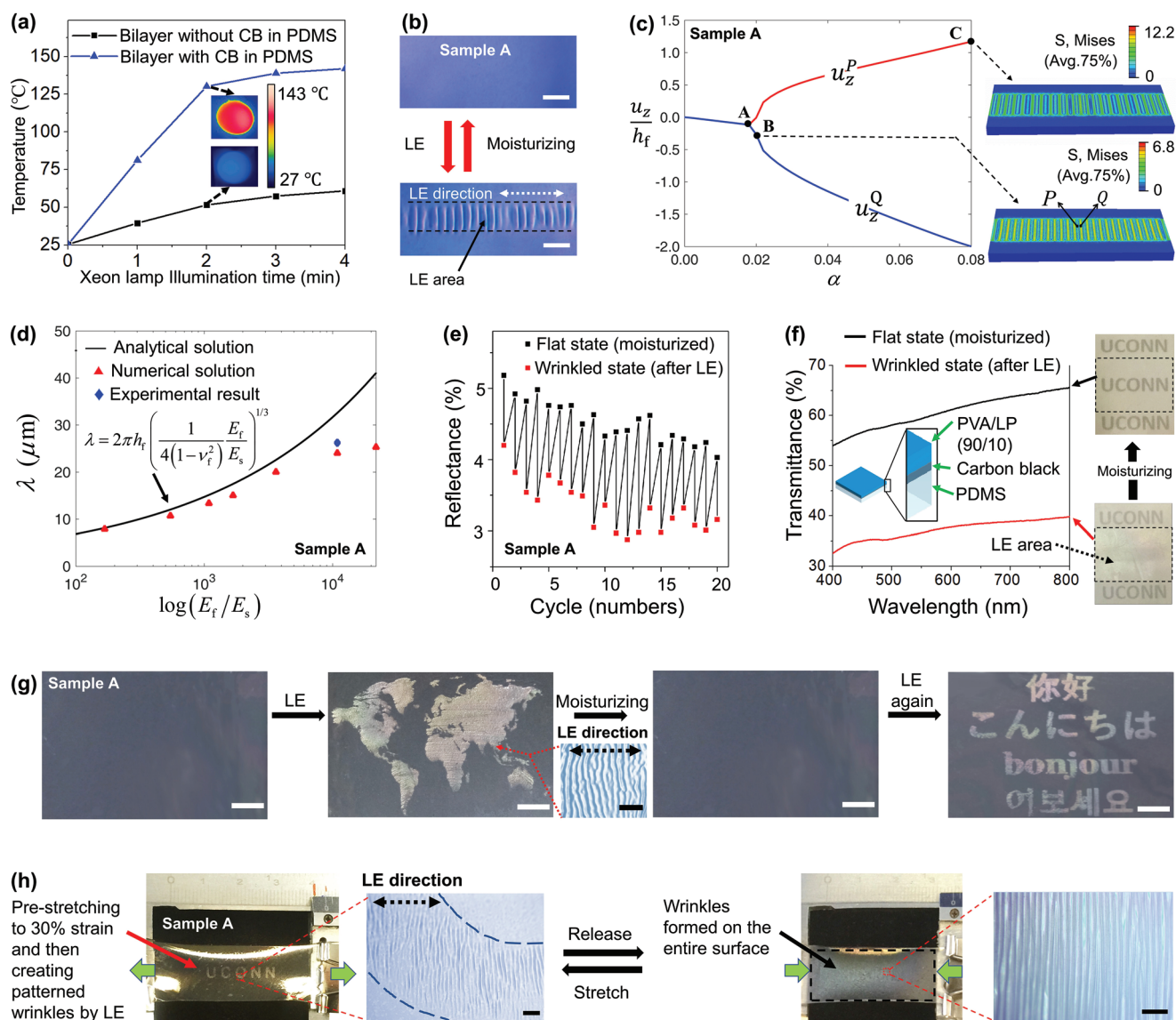


Figure 2. Finite element analysis and characterizations of the LE wrinkles based on Sample A. a) Photothermal effect of the PVA/LP and PDMS bilayer with and without CB in the PDMS matrix. b) Optical microscopic (OM) images of the wrinkles created by laser engraving (LE) and erased by moisture on Sample A (LE power = 1.05 W, scale bar = 100 μm). c) Variation of the vertical displacements u_z at the crest and trough of a wrinkle (points Q and P) on the top surface $z = h_f$ (Figure S7, Supporting Information) by the FEA. Two representative wrinkling morphologies at small and large expansion ratios (points B and C) are shown. d) Wrinkle wavelength with respect to different modulus ratios between the thin film and the substrate. Other parameters are the same as those in Figure 2c. e) Cyclic performance based on reflectance spectra of the LE wrinkles on Sample A when undergoing multiple cycles of LE and moisturization erase. f) Transmittance change of the LE wrinkles as erased by moisture for the modified Sample A with CB at the interface of the PVA/LP and PDMS. g) Performance of the re-writable and moisture erasable LE wrinkle patterns based on Sample A (white scale bar = 10 mm, black scale bar = 100 μm). h) Performance of the patterned LE wrinkles on Sample A with 30% pre-stretching strain, which can be concealed after being released (scale bar = 100 μm).

2.2. Finite Element Analysis and Characterizations of the LE Wrinkles Based on Sample A

The photothermal effect of this film-substrate bilayer system is shown in Figure 2a. Both bilayers with and without CB in PDMS were illuminated by a Xeon lamp (power = 300 W, irradiation distance = 10 cm) and the corresponding surface temperatures as a function of illumination time were recorded by a thermal camera. It is evident that the bilayer containing CB

exhibits a much higher increase in temperature (e.g., 78.6 °C higher after 2 min of illumination) than the counterpart without CB. This can be ascribed to the pronounced photothermal effect from CB,^[51] which is crucial to establish a suitable LE power window for wrinkle formation. As shown in Figure S5 (Supporting Information), if no CB is incorporated, either no wrinkles were generated at power <2.1 W or the film was burnt at power ≥2.1 W. While on Sample A with CB, we observed an aligned wrinkled morphology in the optical microscopy (OM)

image (Figure 2b) generated by a LE power of 1.05 W at a scanning rate of $1.0 \text{ mm}^2 \text{ s}^{-1}$. The width of this wrinkled pattern is $\approx 100 \text{ }\mu\text{m}$, which is the lowest value that can be achieved through this laser engraving process. Figure S6 (Supporting Information) shows that the decrease of LE scanning rate from 1.4 to $1.0 \text{ mm}^2 \text{ s}^{-1}$ can enhance the amplitude of wrinkles from 0.85 to $1.55 \text{ }\mu\text{m}$, due to larger expansion brought by longer laser beam exposure time. No further amplitude increase was observed when the scanning rate was decreased to less than $1.0 \text{ mm}^2 \text{ s}^{-1}$, ascribed to the surface temperature reaching a maximum value upon sufficiently lengthy laser exposure.^[52] As such, $1.0 \text{ mm}^2 \text{ s}^{-1}$ scanning rate was selected for this entire work.

To understand the mechanism for the aligned wrinkles, we conducted FEA to simulate wrinkle formation upon prescribing an isotropic thermal expansion strain α in the film of Sample A (see Experimental Section and Figure S7, Supporting Information). In Figure 2c, when α exceeds a critical value at point A, bifurcation of displacements at the crest and trough of a wave, i.e., u_z^P and u_z^Q , emerges (indicates the wrinkle formation upon the critical thermal strain, as shown for the configurations at points B and C (Figure 2c)). It can be observed that the simulated wrinkle is well-aligned and perpendicular to the laser scanning direction with a wavelength of $\approx 24 \text{ }\mu\text{m}$, which matches well with the corresponding experimental value of $\approx 26.2 \text{ }\mu\text{m}$ (see Figure 2d). Such a unique well-aligned wrinkle morphology is attributed to the anisotropic compressive stress inside the film. As shown in Figure S8a (Supporting Information), both x and y directional stresses, σ_x and σ_y , are negative and σ_x is significantly greater than σ_y for different modulus ratios E_f/E_s , where E_f and E_s are elastic moduli of the film and substrate, respectively. This indicates that the PVA/LP film is in anisotropic compression before wrinkles emerge. Such a stress pattern is due to anisotropic constraints imposed by the surrounding media on the thermal expansion of the film, which is stronger along the scanning direction than in its perpendicular direction. The aligned wrinkled patterns was also observed in a film-substrate strip undergoing uniaxial expansion^[53] (i.e., $\alpha_x = \alpha$, $\alpha_y = 0$), where the stress before wrinkles emerging satisfies $\sigma_x > \sigma_y = 0$. The corresponding critical stress and the wavelength can be obtained by^[54]

$$\sigma_x = \frac{E_f}{4(1-\nu_f^2)} \left(3 \frac{E_s(1-\nu_f^2)}{E_f(1-\nu_s^2)} \right)^{\frac{2}{3}} \quad (1)$$

and

$$\lambda = 2\pi h_f \left(\frac{1}{4(1-\nu_f^2)} \frac{E_f}{E_s} \right)^{\frac{1}{3}} \quad (2)$$

These FEA results for both σ_x and λ agree with the analytical solutions across a large range of modulus ratios (Figure 2d and Figure S8b, Supporting Information), except for the cases with large modulus ratios where the stress anisotropy is not obvious. If an isotropic compressive stress is present in the film, i.e., $\sigma_x = \sigma_y$, a herringbone wrinkled pattern would emerge as the preferable morphology.^[54] In the current system, the x directional

stress was significantly larger than that in the y direction, i.e., $\sigma_x > \sigma_y > 0$, due to the stiffer constrain on the material expansion in the scanning direction. Because of this, the film in the x direction will be squeezed more than in the y direction, leading to the preferred configurations with the aligned wrinkles.

The LE wrinkles in Sample A can be instantaneously erased by moisture and re-engraved by laser for many cycles after drying the area, as characterized by the reflectance changes in multiple moisturization-engraving cycles in Figure 2e. Although Sample A is opaque due to the existence of CB in the PDMS matrix, it can be further modified to possess a decent initial transmittance (62% at 600 nm) in the flat state when much less CB was deposited at the interface of the PVA/LP film and the PDMS substrate (concentration of CB = 0.023 mg cm^{-2}). This modified Sample A also exhibited a decent photothermal effect as compared to that without CB (see Figure S9, Supporting Information). Thus, the LE wrinkles (power = 1.05 W) can be generated concomitant with a decrease of transmittance to 37% at 600 nm, and it can be rapidly and reversibly erased by moisture within 5 s (see Figure 2f and Figure S10, Supporting Information). In terms of application, Sample A can be leveraged for a moisture erasable and laser re-writable wrinkles-based patterning surface (see Figure 2g and Movie S1, Supporting Information). Additionally, if a moisturized Sample A was pre-stretched to 30% strain prior to drying, the dried sample could be used to generate aligned LE wrinkled patterns (LE power = 1.05 W, using “UCONN” logo as an example) as shown in Figure 2h. Since the PVA/LP thin film is incompressible, when Sample A is totally released, the PDMS substrate exerts a compressive force to the entire thin film layer. Herein, new aligned wrinkles were generated on the entire thin film surface when released, which concealed the original “UCONN” patterned LE wrinkles in both micro and macro-scale. And these hidden LE wrinkles can be revealed again upon re-stretching Sample A to 30% strain. Thus, these wrinkled devices based on Sample A provide intriguing demonstrations for applications in recording or encryption of the moisture/photo/mechanical responsive information.

2.3. Characterizations and Performance of the Two Types of LE Wrinkles Based on Sample B

In Sample B, as shown in Figure 3a, the peeling process created distributed aligned cracks on the brittle film due to the higher concentration (40 wt%) of LP (as noted above, no cracks will form on Sample A because its PVA film contains a low LP concentration (10 wt%) and thus is sufficiently ductile), which gave rise to a highly anisotropic compressive stress during the photothermal induced expansion process, because the constraints on the expansion were anisotropic in the crack lines. This strong physical confinement effect can lead to vertical alignment of LE wrinkles (wavelength = $35 \text{ }\mu\text{m}$, amplitude = $1.55 \text{ }\mu\text{m}$, at LE power = 1.05 W, see Figure S11, Supporting Information) to the cracking direction.^[37,55,56] To generate LE wrinkles that are less sensitive to moisture, PVA (POVAL 28–99) with a high DH of $\approx 99\%$ was chosen for this purpose. PVA (POVAL 28–99) exhibits a much higher crystallinity, making it much more resistant to moisture compared to

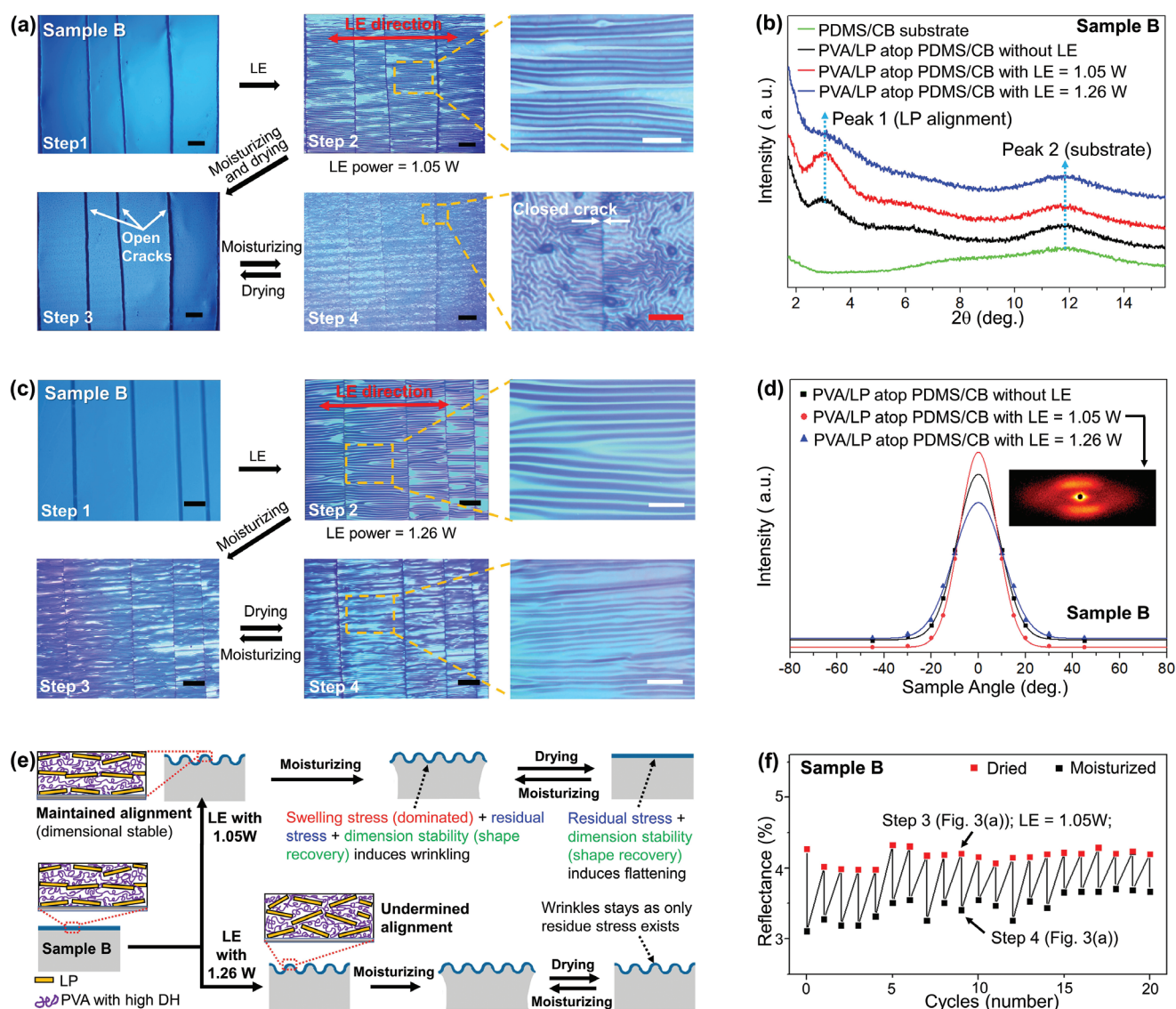


Figure 3. Characterizations and performance of the LE wrinkles based on Sample B engraved by different LE powers. a) OM images of the moisture responsiveness of the wrinkles generated by LE power = 1.05 W on Sample B (black scale bar = 200 μm , white scale bar = 100 μm , red scale bar = 50 μm). b) XRD patterns of the PDMS/CB substrate, and the PVA/LP layer on Sample B without/with LE under different powers. c) OM images of the moisture responsiveness of the wrinkles generated by LE power = 1.26 W on Sample B (black scale bar = 200 μm , white scale bar = 100 μm). d) Scattering intensity as a function of sample angle for incident beam in the small-angle X-ray scattering (SAXS), where the solid line is fitted. e) Proposed mechanism of the moisture responsive dynamics of the wrinkling surface on Sample B under different LE powers. f) Cyclic performance based on reflectance spectra of the wrinkles created by LE = 1.05 W power on Sample B when undergoing multiple moisturization and drying cycles.

the partially hydrolyzed PVA (POVAL 8–88) used for Sample A (see Figure S4 in the Supporting Information). This was confirmed by the control bilayer structure consisting of pure PVA (POVAL 28–99) and PDMS/CB, on which the LE wrinkles could only be partially released by moisture (see Figure S12 in the Supporting Information). Meanwhile, the nacre-like LP alignment (also evident in the TEM image in Figure 1c) in the PVA/LP film is confirmed by the X-ray diffraction (XRD) pattern in Figure 3b, which shows an intense basal diffraction peak at 2.9° (labeled as Peak 1, where Peak 2 belongs to the substrate) in the XRD pattern of the PVA/LP film before LE.^[36] Notably, after a 1.05 W LE power was applied, a slightly more intense peak at the same position is observed, indicating that the LP nanosheet

alignment was marginally improved. Herein, the mild photo-thermal effect under LE = 1.05 W can induce movement of PVA chains, which is favorable for the alignment of LP nanosheets, similar to the thermal annealing processing.^[57,58] Therefore, in the PVA/LP film layer, the well-aligned LP nanosheets play a key role as “hard segments” that improve dimensional stability at molecular-/nano-scale and serve as physical crosslinking points for shape recovery,^[44–46,48,49,59] while the PVA chains act as “soft segments” that are deformable under photothermal effect. As this wrinkled surface was exposed to moisture, only part of the stress created during the LE process on this area was released, due to the high moisture resistance of PVA, and thus partial residual stress remained. In this moisturization step,

although the shape recovery effect originating from the dimensional stability induced by the aligned LP nanosheets tended to re-flatten the surface, it failed to compete with the moisture induced swelling stress and the residual stress, as a result these two variables enabled the presence of wrinkles at a wet state. However, upon being dried, the shape recovery effect overcame the residual stress and effectively restricted the motion of PVA chains, enabling the release of the microscale LE wrinkles into a flattened surface. During re-moisturization, the residual stress combined with the swelling stress again collectively generated wrinkles on the original LE area. Note that no wrinkles can be formed upon moisturization if the surface did not undergo LE treatment, because only swelling stress without residual stress from LE process was not sufficient to generate wrinkles. Therefore, as shown in Figure 3a, upon re-moisturization, the labyrinth patterned wrinkled surface attributed to the isotropic swelling stress^[53] (wavelength = 9.5 μm ; amplitude = 401 nm) was generated on the original LE area and it was re-flattened after dried. It is worth mentioning that the open cracks in Step 3 in Figure 3a can close concomitant with the wrinkle formation (Step 4 in Figure 3a) during the following moisturization cycle (also see Movie S2, Supporting Information) due to the swelling effect. This collective actuation of cracks and wrinkles upon moisturization inspire the design of novel moisture responsive electrical switch, in which the open/close of the cracks can function as an electrical switch and the concomitant wrinkle formation/disappearance can be used as optical signals to indicate the working status of the switch.

If a high LE power = 1.26 W is used, similar aligned wrinkles (wavelength = 47 μm ; amplitude = 1.5 μm , as shown in Figure 3c) can also be generated but demonstrate undermined LP alignment. This is because the PVA chains experience significantly large deformations when they are heated by this high LE power, and the random chain movement disrupts the LP nanosheet orientation, undermining the LP alignment. As shown in Figure 3b, the peak at $\approx 2.9^\circ$ almost disappeared. This effect was further investigated by small angle X-ray scattering (SAXS). Figure S13 (Supporting Information) shows the SAXS patterns around the Bragg angle ($q \approx 0.21 \text{ \AA}^{-1}$) under different incident beam angles to the PVA/LP film. To quantitatively analyze the LP alignment, the intensity at the Bragg angle as a function of incident beam angle was plotted and fitted as shown in Figure 3d, which shows that the full width at half maximum (FWHM) of the fitting curves of the PVA/LP with LE = 1.05 W, without LE, and with LE = 1.26 W are 18.7° , 21.2° , and 24.7° , respectively. A higher FWHM indicates a lower degree of overall alignment, which is consistent with the XRD result. In this case, the LP nanosheets are not able to effectively restrict the motion of the PVA chains and thus the shape recovery effect is significantly undermined. Therefore, the wrinkled surface was only partially released as dried from moisturization (wavelength = 18 μm , amplitude = 536 nm after being moisturized), which exhibited a similar moisture response as the pure PVA (see Figure S12 in the Supporting Information). The moisture responsive dynamics of the wrinkles on Sample B under LE = 1.05 and 1.26 W are summarized in Figure 3e, which demonstrates that the LE process can not only generate microscale wrinkles, but also tailor the LP alignment in the film by varying the laser power, and the change

of this nanoarchitecture eventually determines the moisture responsiveness of the wrinkles. Additionally, as shown in Figure 3f, the wrinkles in Sample B maintain excellent reversibility as treated by LE = 1.05 W over multiple moisturization and drying cycles.

2.4. Moisture Responsive Anti-Counterfeit Device and Moisture Responsive Electrical Switch Based on Sample B

A moisture responsive anti-counterfeit device based on Sample B was developed. As shown in Figure 4a, Sample B was subject to LE with 1.26 and 1.05 W on different areas of a QR code pattern. Upon being moisturized and dried, the original LE area with 1.05 W beam was re-flattened, while the wrinkled area engraved by 1.26 W beam maintained visible with the word "MOISUTRE" exhibited. Thus, to reveal the QR code hidden on the original LE area with 1.05 W beam, moisturization (such as through breathing) is needed to activate the wrinkles, and it re-flattens again once dried (also see Movie S3, Supporting Information). Additionally, a moisture responsive electrical switch based on Sample B was designed and is shown in Figure 4b. Sample B was further modified with a thin electrically conductive PEDOT: PSS/PVA layer deposited atop the PVA/LP film with only half of the sample area treated by a LE power of 1.05 W. The LE area was moisturized and dried prior to being connected to a LED lamp and a power source. Hence, the LE area is flattened with open cracks and is in a non-conductive state when dried. Upon moisturization, wrinkles form on the LE area concomitant with the closing of the cracks due to the swelling stress, which allows this area to exhibit reflectance/brightness changes due to the wrinkle formation and become conductive to turn on the LED lamp as the crack closed. As shown in Figure 4c, after moisturization, the initial high resistance ($\approx 5.06 \times 10^3 \text{ M}\Omega$) of the LE area dropped drastically to $\approx 595 \text{ k}\Omega$ due to the crack closing, concomitant with the dramatic change in the brightness from $\approx 29\%$ to $\approx 55\%$ due to the wrinkle formation within 5 s, which acts as a diffuse reflector (also see Movie S4, Supporting Information). The device demonstrates an excellent reversibility after many cycles of moisturization and drying. Note that the abrupt change at $\approx 18 \text{ M}\Omega$ was shown on the curves for resistance evolution, attributed to the crack opening at the drying cycle or the crack closing at moisturization cycle, respectively. The RH response of this system is shown in Figure S14 (Supporting Information), and the resistance drastically decreased when the RH increased up to 80%, accompanied with a dramatic increase in brightness.

3. Conclusion

In summary, we developed a dynamic, versatile, convertible, and responsive laser writable wrinkled system, which was realized by a multiscale photo/moisture reconstructible hybrid structure composed of a PVA/LP film and a PDMS/CB substrate. The spatiotemporally controllable laser was not only used to generate programmable aligned wrinkles but also applied to tailor the morphology of the LP nanosheets in the PVA/LP film. The FEA showed that the formation of

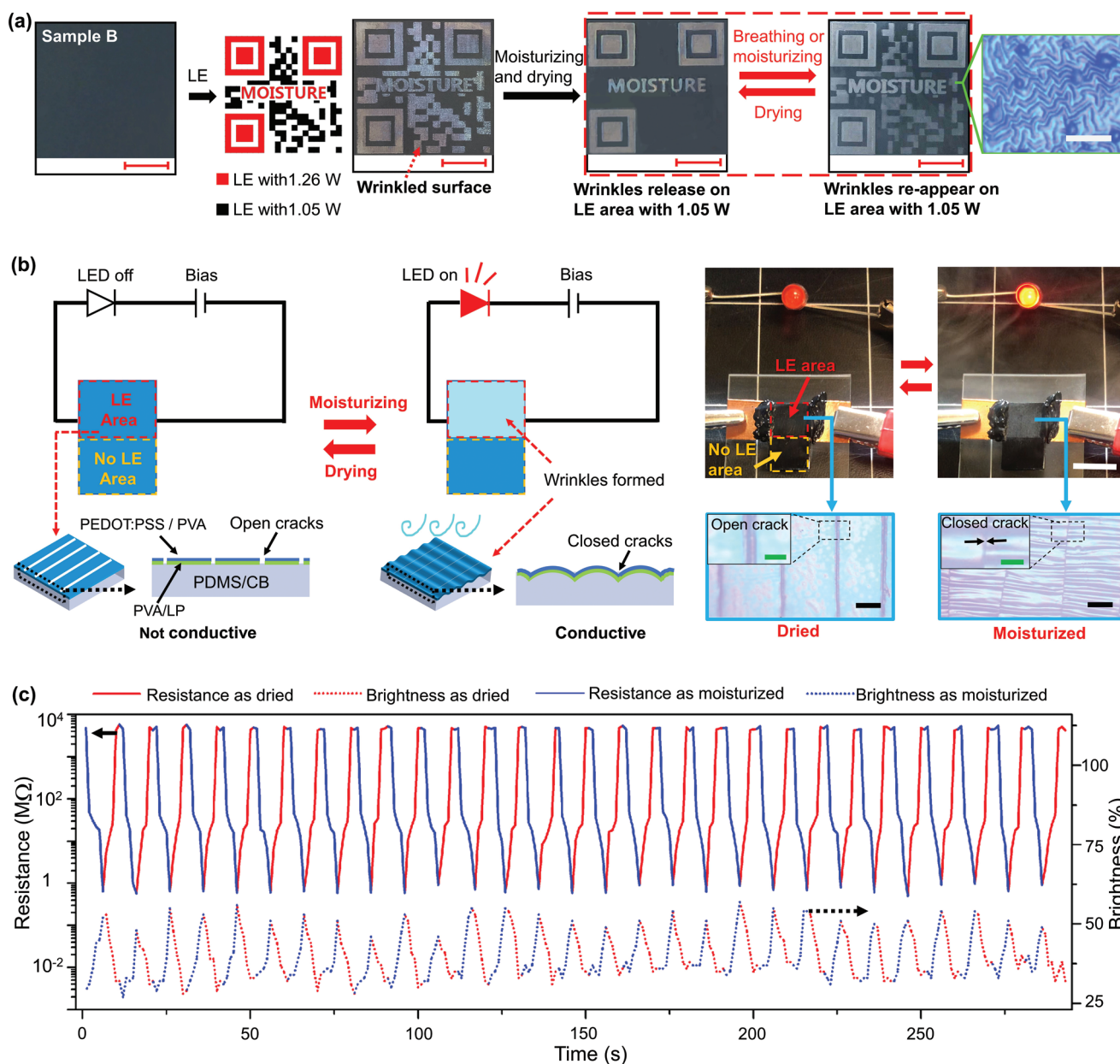


Figure 4. Moisture responsive encryption device and moisture responsive electrical switch based on Sample B. a) Schematic and performance of Sample B applied for a moisture responsive encryption device (red scale bar = 8.3 mm, white scale bar = 50 μm). b) Schematic and performance of the modified Sample B with a PEDOT: PSS top layer applied for moisture responsive electrical switch (white scale bar = 1 cm, black scale bar = 100 μm, green scale bar = 30 μm). c) Reversibility of the moisture responsive resistance and brightness of the LE area on the modified Sample B when undergoing multiple moisturization and drying cycles.

aligned wrinkles originated from the anisotropic stress generated by the mismatched film-substrate expansion and the concomitant surrounding constraints. To modulate the moisture responsiveness of the laser generated wrinkles, the DH of PVA, the ratio of LP to PVA, and laser power were carefully tuned for two structural designs named as Samples A and B. In Sample A, the film contains low DH PVA (≈88%) and a low LP concentration (10 wt%). Thus, LE wrinkles can be readily erased by moisture and re-engraved by another LE cycle, which can be applied for moisture/photo/mechanical

responsive information encryption/recording devices. A modified Sample A with high initial transparency can also be fabricated. In Sample B, the thin film is comprised of a high DH PVA (≈99%) and a high LP concentration (40 wt%), which results in a topography with distributed cracks and nacre-like LP alignment in the film. Under a 1.05 W LE power, the LE wrinkles formed while maintaining the alignment of LP. This endowed the thin film with high dimensional stability and good shape recovery effect, which competed with the swelling stress during moisturization and residual stress originating

from the LE process, to collectively determine the wrinkles' presence and/or disappearance. Herein, the wrinkles can be reversibly activated by further moisturization on the original LE area, concomitant with closing of open cracks. For the wrinkles generated by a 1.26 W LE power, the alignment of the LP was undermined and dimensional stability impaired, inducing the film with moisture resistant wrinkles. Herein, these novel properties enabled the invention of a moisture responsive encryption device and a moisture responsive electrical switch based on Sample B. Note that this switch can also be used as a RH sensor coupling optical and electrical signals. Since the wrinkled surface effectively scatters a much wider angle of light compared to the flattened counterpart due to its periodical microscale structure,^[11] this system can be further applied as a light diffusor, anti-glare surface, and broaden viewing angles for structural color devices. This work focuses on various structural and fabrication elements, ranging from formulating polymer molecular structure to constructing micro/nano-scale architecture to fabricate macroscale film-substrate bilayer structure. It offers a compelling example on how the multiscale and multi-level variables can collectively and interactively determine the generation of the LE wrinkles and the modulation of the moisture responsive dynamics of wrinkles, serving as a remarkable guidance for future development of multifunctional responsive smart materials with wider scope of applications.

4. Experimental Section

Preparation of Sample A: As shown in Figure S3 (Supporting Information), a polyvinyl alcohol (PVA) and laponite (LP) composite film (mass ratio of PVA to laponite = 9:1) with a thickness of ≈ 350 nm was cast on a pre-cleaned polystyrene petri-dish foundation followed by the treatment of allyl isocyanate (from Alfa Aesar). The chosen PVA grade was POVAL 8–88 ($M_w \approx 67\,000$, degree of hydrolysis (DH) $\approx 88\%$) obtained from KURARAY, Inc. The LP was acquired from BYK Additives Inc. A sample of 5.0 mg mL^{-1} PVA/LP aqueous dispersion was used for casting. Subsequently, a mixture of liquid polydimethylsiloxane (PDMS, Sylgard 184, base to curing agent ratio = 30:1) precursor and carbon black (CB, particle size 30–50 nm, from Alfa Aesar, mass ratio of PDMS to CB = 133:1) was cast atop the allyl isocyanate treated PVA/laponite film followed by cooling down to -10°C in a freezer overnight to allow PDMS to thoroughly penetrate into the film to create a strong interface. The sample was then cured at 80°C for 4 h to form a soft solid sheet with a thickness of ≈ 1 mm. This bilayer sheet was then carefully peeled away from the foundation in one direction. Subsequently, a laser engraver (Niotech 3000 mW Mini desktop laser engraver machine) was used with a designated power at a scanning rate of $1.0\text{ mm}^2\text{ s}^{-1}$ to generate wrinkled patterns. Note that the top surface of the sample is exposed to the laser source at a distance of 8 cm.

Preparation of a Modified Sample A with High Transparency: The casting of PVA/LP composite film atop the polystyrene petri-dish and the allyl isocyanate treatment is the same as aforementioned. Subsequently, a thin layer of CB (concentration of CB = 0.023 mg cm^{-2}) is applied atop the PVA/LP surface via spray-coating by an airbrush style spray-gun (Master Airbrush G444-SET, needle nozzle 0.5 mm and Royal Mini Air Compressors, TC-20B). A layer of liquid PDMS precursor (base to curing agent ratio = 30:1) was then cast atop the carbon black surface followed by cooling down to -10°C in a freezer overnight. The sample was then cured at 80°C for 4 h to form a soft solid sheet with thickness of ≈ 1 mm. The cured sample sheet was then carefully peeled away from the foundation in one direction.

Preparation of Sample B: The preparation of Sample B was the same as Sample A except for using KURARAY POVAL 28–99 ($M_w \approx 145\,000$, DH $\approx 88\%$) as the PVA matrix and a different mass ratio of PVA to LP = 6:4.

Preparation of a Modified Sample B for Moisture Responsive Electrical Switch: A layer of PEDOT: PSS/PVA (PEDOT: PSS obtained from Sigma Aldrich) with a thickness of ≈ 235 nm was cast on Sample B surface (mass ratio of PEDOT: PSS to PVA (POVAL 28–99) = 6:4, and 5.0 mg mL^{-1} aqueous solution was used). The resultant sample was cut into a size of $8\text{ mm} \times 16\text{ mm}$ and half of area underwent a laser engraving (LE) power of 1.05 W to generate wrinkles, as shown in Figure 4b. Subsequently, the sample was moisturized and then dried to flatten the LE wrinkles followed by electrically connected to an LED lamp and a power source.

Finite Element Analysis (FEA) of the LE Wrinkles on Sample A: Since the length of the PVA/LP and PDMS in Sample A is much larger than the width of the wrinkling area, a part of the structure was taken and the x-directional displacements were constrained at $x = l_0/2$ and $-l_0/2$, and all degrees of freedom at the bottom surface $z = -h_s$, where l_0 is the total length of the simulation domain, and h_s is the thickness of the PDMS substrate (see Figure S7 in the Supporting Information). The material and geometrical parameters in the simulation are taken from the experiments, where $h_f = 0.35\text{ }\mu\text{m}$, $h_s = 20\text{ }\mu\text{m}$, $l_0 = 480\text{ }\mu\text{m}$, $w_0 = \frac{w_1}{2} = 40\text{ }\mu\text{m}$, $E_s = 0.1\text{ Mpa}$, $E_f = 1090\text{ Mpa}$, $\nu_f = 0.4$, and $\nu_s = 0.49$. E and ν are elastic modulus and Poisson's ratio, respectively, and the quantities with subscripts "s" and "f" denote those of PDMS substrate and PVA film, respectively. Abaqus 6.9 was used to simulate this problem, where the isotropic thermal expansion of PVA, $\alpha_x = \alpha_y = \alpha_z = \alpha$, was directly applied in the scanned area to trigger the deformation of the entire structure. The convergence study was performed to ensure the accuracy of simulation results.

Characterization: The TEM images of the PVA/LP films were captured on a JEOL 2010 FASTEM transmission electron microscope. The photothermal effect of the samples was tested under the illumination of a 300 W Xenon lamp (Newport Corporation) for specific durations and the corresponding temperatures were recorded by a FLIR E5-XT IR camera. The optical microscopic images were taken by an AmScope ME 520TA microscope under reflective mode. The reflectance spectra were recorded by a Mprobe VIS-NIR thin film measurement system. The UV–vis transmittance spectra were recorded by a Perkin Elmer ultraviolet/visible/near-infrared Lambda 900 spectrophotometer. The amplitudes of the wrinkles were tested on a ZYGO NewView 5000 non-contact white-light profilometer. Small-angle X-ray scattering (SAXS) analysis was conducted on a Bruker NanoSTAR instrument. The wide-angle XRD patterns were recorded on a Bruker D8 diffractometer. The resistance of the moisture responsive electrical switch was measured by a Keithley 2400 Source Measure Unit. The brightness of the LE area on the moisture responsive electrical switch was captured by a digital camera and analyzed by the Photoshop Express.

Supporting Information

Supporting Information is available from the Wiley Online Library or from the author.

Acknowledgements

The authors thank Kuraray for providing the polyvinyl alcohol samples and thank Dr. Yuntao Li for helpful discussions. A.T.S. acknowledges the GAANN Fellowship (No. P200A150330).

Conflict of Interest

The authors declare no conflict of interest.

Keywords

dynamic micropatterns, multiscale structure, smart materials, stimuli responsive materials, wrinkles

Received: November 9, 2020

Revised: November 25, 2020

Published online:

- [1] F. T. Malik, R. M. Clement, D. T. Gethin, W. Krawszik, A. R. Parker, *Bioinspir. Biomim.* **2014**, 9, 031002.
- [2] A. R. Parker, C. R. Lawrence, *Nature* **2001**, 414, 33.
- [3] P. J. Bentley, W. F. C. Blumer, *Nature* **1962**, 194, 699.
- [4] P. Comanns, C. Effertz, F. Hischen, K. Staudt, W. Böhme, W. Baumgartner, *Beilstein J. Nanotechnol.* **2011**, 2, 204.
- [5] R. T. Hanlon, C.-C. Chiao, L. M. Mäthger, A. Barbosa, K. C. Buresch, C. Chubb, *Philos. Trans. R. Soc., B* **2009**, 364, 429.
- [6] Y. Li, X. Bai, T. Yang, H. Luo, C.-W. Qiu, *Nat. Commun.* **2018**, 9, 273.
- [7] S. Zeng, D. Zhang, W. Huang, Z. Wang, S. G. Freire, X. Yu, A. T. Smith, E. Y. Huang, H. Nguon, L. Sun, *Nat. Commun.* **2016**, 7, 11802.
- [8] S. Zeng, H. Sun, C. Park, M. Zhang, M. Zhu, M. Yan, N. Chov, E. Li, A. T. Smith, G. Xu, S. Li, Z. Hou, Y. Li, B. Wang, D. Zhang, L. Sun, *Mater. Horiz.* **2020**, 7, 164.
- [9] H. M. Whitney, B. J. Glover, R. Walker, A. G. Ellis, *Curtis's Bot. Mag.* **2011**, 28, 349.
- [10] H. Hou, J. Yin, X. Jiang, *Acc. Chem. Res.* **2019**, 52, 1025.
- [11] S. Zeng, R. Li, S. G. Freire, V. M. M. Garbellotto, E. Y. Huang, A. T. Smith, C. Hu, W. R. T. Tait, Z. Bian, G. Zheng, D. Zhang, L. Sun, *Adv. Mater.* **2017**, 29, 1700828.
- [12] Z. Ma, J. Zhou, J. Zhang, S. Zeng, H. Zhou, A. T. Smith, W. Wang, L. Sun, Z. Wang, *Mater. Horiz.* **2019**, 6, 2003.
- [13] S. Chen, S. Zeng, S. Liu, H. Liu, R. Zheng, K. L. White, A. T. Smith, L. Liu, L. Sun, *Chem. Mater.* **2019**, 31, 8708.
- [14] M. Guo, Y. Wu, S. Xue, Y. Xia, X. Yang, Y. Dzenis, Z. Li, W. Lei, A. T. Smith, L. Sun, *J. Mater. Chem. A* **2019**, 7, 25969.
- [15] S. Chen, H. Liu, S. Liu, P. Wang, S. Zeng, L. Sun, L. Liu, *ACS Appl. Mater. Interfaces* **2018**, 10, 4305.
- [16] C. Wu, S. Zeng, Z. Wang, F. Wang, H. Zhou, J. Zhang, Z. Ci, L. Sun, *Adv. Funct. Mater.* **2018**, 28, 1803168.
- [17] X. Su, H. Li, X. Lai, L. Zheng, Z. Chen, S. Zeng, K. Shen, L. Sun, X. Zeng, *ACS Appl. Mater. Interfaces* **2020**, 12, 14578.
- [18] A. T. Smith, H. Ding, A. Gorski, M. Zhang, P. A. Gitman, C. Park, Z. Hao, Y. Jiang, B. L. Williams, S. Zeng, A. Kokkula, Q. Yu, G. Ding, H. Zeng, L. Sun, *Matter* **2020**, 2, 680.
- [19] C. S. Davis, D. Martina, C. Creton, A. Lindner, A. J. Crosby, *Langmuir* **2012**, 28, 14899.
- [20] Y. Rahmawan, C.-M. Chen, S. Yang, *Soft Matter* **2014**, 10, 5028.
- [21] J. Cong, J. Wang, J. Xie, C. Yang, J. Zhao, L. Li, Y. Cao, A. Fery, X.-Q. Feng, C. Lu, *Langmuir* **2018**, 34, 4793.
- [22] L. Qi, C. Ruck, G. Spychalski, B. King, B. Wu, Y. Zhao, *ACS Appl. Mater. Interfaces* **2018**, 10, 4295.
- [23] C. Zong, Y. Zhao, H. Ji, X. Han, J. Xie, J. Wang, Y. Cao, S. Jiang, C. Lu, *Angew. Chem., Int. Ed.* **2016**, 55, 3931.
- [24] Y. Jiang, S. Zeng, Y. Yao, S. Xu, Q. Dong, P. Chen, Z. Wang, M. Zhang, M. Zhu, G. Xu, H. Zeng, L. Sun, *Polymers* **2019**, 11, 103.
- [25] Z. Mao, S. Zeng, K. Shen, A. P. Chooi, A. T. Smith, M. D. Jones, Y. Zhou, X. Liu, L. Sun, *Adv. Opt. Mater.* **2020**, 2001472, <https://doi.org/10.1002/adom.202001472>.
- [26] Y. Xu, S. Zeng, W. Xian, L. Lin, H. Ding, J. Liu, M. Xiao, S. Wang, Y. Li, Y. Meng, L. Sun, *Macromol. Rapid Commun.* **2020**, 2000446, <https://doi.org/10.1002/marc.202000446>.
- [27] Z. Chen, G. Huang, I. Trase, X. Han, Y. Mei, *Phys. Rev. Appl.* **2016**, 5, 017001.
- [28] P.-C. Lin, S. Yang, *Soft Matter* **2009**, 5, 1011.
- [29] J. Lin, Q. Guo, S. Dou, N. Hua, C. Zheng, Y. Pan, Y. Huang, Z. Chen, W. Chen, *Extreme Mech. Lett.* **2020**, 36, 100653.
- [30] S. Zeng, R. Li, W. R. T. Tait, A. T. Smith, M. Zhang, M. Zhu, N. Chov, G. Xu, D. Zhang, L. Sun, *Mater. Horiz.* **2020**, 7, 1288.
- [31] C. Zong, U. Azhar, C. Zhou, J. Wang, L. Zhang, Y. Cao, S. Zhang, S. Jiang, C. Lu, *Langmuir* **2019**, 35, 2601.
- [32] J. Wang, Y. Zheng, L. Li, E. Liu, C. Zong, J. Zhao, J. Xie, F. Xu, T. A. F. König, M. Grenzer Saphiannikova, Y. Cao, A. Fery, C. Lu, *ACS Appl. Mater. Interfaces* **2019**, 11, 25595.
- [33] C. Zong, Y. Zhao, H. Ji, J. Xie, X. Han, J. Wang, Y. Cao, C. Lu, H. Li, S. Jiang, *Macromol. Rapid Commun.* **2016**, 37, 1288.
- [34] P. Gruner, M. Arlt, T. Fuhrmann-Lieker, *ChemPhysChem* **2013**, 14, 424.
- [35] H. Hou, F. Li, Z. Su, J. Yin, X. Jiang, *J. Mater. Chem. C* **2017**, 5, 8765.
- [36] F. Ding, J. Liu, S. Zeng, Y. Xia, K. M. Wells, M.-P. Nieh, L. Sun, *Sci. Adv.* **2017**, 3, 1701212.
- [37] L. Zhou, T. Ma, T. Li, X. Ma, J. Yin, X. Jiang, *ACS Appl. Mater. Interfaces* **2019**, 11, 15977.
- [38] F. Li, H. Hou, J. Yin, X. Jiang, *Sci. Adv.* **2018**, 4, eaar5762.
- [39] C. Qu, S. Wang, L. Liu, Y. Bai, L. Li, F. Sun, M. Hao, T. Li, Q. Lu, L. Li, S. Qin, T. Zhang, *Small* **2019**, 15, 1900216.
- [40] S. Zhou, M. Wang, J. Yang, F. Xu, *RSC Adv.* **2015**, 5, 35976.
- [41] H. Z. Cummins, *J. Non-Cryst. Solids* **2007**, 353, 3891.
- [42] Y. Xu, Y. Zhou, J. Liu, L. Sun, *J. Energy Chem.* **2017**, 26, 1026.
- [43] I. M. Hutten, in *Handbook of Nonwoven Filter Media*, 2nd ed. (Ed: I. M. Hutten), Butterworth-Heinemann, Oxford **2016**, p. 263.
- [44] G. Du, A. Mao, J. Yu, J. Hou, N. Zhao, J. Han, Q. Zhao, W. Gao, T. Xie, H. Bai, *Nat. Commun.* **2019**, 10, 800.
- [45] Q. Wu, D. Guo, Y. Zhang, H. Zhao, D. Chen, J. Nai, J. Liang, X. Li, N. Sun, L. Guo, *ACS Appl. Mater. Interfaces* **2014**, 6, 20597.
- [46] W. Xing, B. Yuan, X. Wang, Y. Hu, *Mater. Des.* **2017**, 115, 46.
- [47] J. Mendez, P. K. Annamalai, S. J. Eichhorn, R. Rusli, S. J. Rowan, E. J. Foster, C. Weder, *Macromolecules* **2011**, 44, 6827.
- [48] A. Knöller, C. P. Lampa, F. v. Cube, T. H. Zeng, D. C. Bell, M. S. Dresselhaus, Z. Burghard, J. Bill, *Sci. Rep.* **2017**, 7, 40999.
- [49] S. Liu, F. Yao, O. Oderinde, K. Li, H. Wang, Z. Zhang, G. Fu, *Chem. Eng. J.* **2017**, 321, 502.
- [50] B. Liang, H. Zhao, Q. Zhang, Y. Fan, Y. Yue, P. Yin, L. Guo, *ACS Appl. Mater. Interfaces* **2016**, 8, 28816.
- [51] R. Jiang, S. Cheng, L. Shao, Q. Ruan, J. Wang, *J. Phys. Chem. C* **2013**, 117, 8909.
- [52] B. Zhu, M. Noack, R. Merindol, C. Barner-Kowollik, A. Walther, *Nano Lett.* **2016**, 16, 5176.
- [53] B. Audoly, A. Boudaoud, *J. Mech. Phys. Solids* **2008**, 56, 2401.
- [54] X. Chen, J. W. Hutchinson, *J. Appl. Mech.* **2004**, 71, 597.
- [55] H. Vandeparre, S. Desbief, R. Lazzaroni, C. Gay, P. Damman, *Soft Matter* **2011**, 7, 6878.
- [56] W. Ding, Y. Yang, Y. Zhao, S. Jiang, Y. Cao, C. Lu, *Soft Matter* **2013**, 9, 3720.
- [57] A. A. Umar, S. K. Md Saad, M. M. Salleh, *ACS Omega* **2017**, 2, 3325.
- [58] I. Roy, S. Hazra, *RSC Adv.* **2015**, 5, 665.
- [59] X. Qi, X. Yao, S. Deng, T. Zhou, Q. Fu, *J. Mater. Chem. A* **2014**, 2, 2240.